16th World Conference on Earthquake, 16WCEE 2017

Santiago Chile, January 9th to 13th 2017

Paper N° 2291

Registration Code: S-Z1461969442

SENSITIVITY OF SYNTHETIC SEISMOGRAMS FOR DIFFERENT SEISMIC SCENARIOS IN NORTH CHILE

C. Fortuno[(1)], J.C. de la Llera[(2)], G. González[(3)], J. González[(4)], P. Aguirre[(5)]

[(1)] *Researcher,* National Research Center for the *Integrated Management of Natural Disaster (CIGIDEN) CONICYT/FONDAP/15110017, Pontificia Universidad Catolica de Chile,* catalina.fortuno@cigiden.cl

[(2)] *Principal Investigator, CIGIDEN, Pontificia Universidad Catolica de Chile,* jcllera@ing.puc.cl

[(3)] *Principal Investigator, CIGIDEN, Universidad Católica del Norte,* ggonzale@ucn.cl

[(4)] *Researcher, CIGIDEN, Universidad Católica del Norte,* juan.gonzalez@cigiden.cl

[(5)] *Researcher, CIGIDEN, Pontificia Universidad Catolica de Chile,* paula.aguirre@cigiden.cl

Abstract

This research studies the sensitivity of spectral response values to various physical earthquake scenario parameters, the latter used to generate synthetic low frequency seismograms in North Chile. Ten earthquake scenarios have been defined using seed information from the slip model of the 2010, Maule earthquake, and different physically plausible interplate locking models in the region. Firstly, the Maule 2010 finite fault rupture model was resituated in the existing seismic gap in north Chile using a curved geometry according to the Slab 1.0 model. From this seed model, one synthetic scenario with constant moment magnitude M_w 8.8 was generated with the same slip distribution as the original 2010 slip model. Three other models with variations in the slip distribution were considered. In addition, three physically plausible fault rupture models based on previous studies of interplate locking were used. Each of these scenarios was capable of generating M_w 8.2 – 8.4 earthquakes with a maximum slip of 7.5 m, approximately. Patches of major slip were located along the coast line approximately in front of the cities of Arica, Iquique, and Tocopilla, respectively. Also, three additional scenarios with moment magnitudes in the range M_w 8.5 – 8.7 were built by connecting these physical scenarios into larger rupture areas. These combined interplate locking models represented the activation of two or more asperities, similar to the experience of the 2010 Maule earthquake. Using these scenarios we built low frequency synthetic seismograms at four control sites: Arica, Iquique, Tocopilla, and Calama. The sensitivity of these results was studied by deterministic analyses on some key rupture parameters, such as mean rupture velocity and slip rise-time. Sensitivity analysis used peak ground displacement (PGD) and acceleration (PGA), pseudo-acceleration spectra, S_a, and displacement spectra, S_d. The range of values considered for mean rupture velocity was v_r = 2.2-3.0 km/s. Four points were considered in the vicinity of each specified velocity to compute sensitivities. First and second order derivatives of PGD, PGA, S_d, and S_a relative to the source parameters were then used to build a Taylor series expansion to predict PGD, S_a and S_d as a function of v_r. This allows to consider uncertainty in this parameter and propagate such uncertainty into spectral response values. An analogous procedure was considered for rise-time t_r in the range from 2 to 10s.

Keywords: synthetic scenarios, low frequency ground motions, seismic coupling, spectral response

1. Introduction

In spite of the advances in our knowledge in strong ground motion seismology, future seismic scenarios are still highly unpredictable. These different scenarios definitely induce very different ground motions, which are needed to design structures. Because of this uncertainty in design, the aim of this study is to select a number of possible scenarios and evaluate the uncertainty generated in the ground motions at specific sites. The geographical seismic context used is the gap in North Chile. This study only addresses the low-frequency component of the generated ground motions, which may influence more long-period structures. The seismic scenarios considered are a combination of physically plausible scenarios, with others that correspond to previous earthquakes, in particular the Maule (Chile) earthquake in 2010. The rationale behind the selection of the latter is only under the aim of bounding uncertainty, and due to the fact that it already happened with a moment magnitude close to the one expected in the North. These scenarios are the base to build different slip distributions while maintaining similar rupture global parameters such as geometry and magnitude. Based on these scenarios, a parametric analysis was made to evaluate the effect of key rupture parameters on the design ground motions. Consequently, spectral responses were used to monitor these effects at four control sites.

The methodology used herein uses two rupture families as a base of slip models: (i) the 2010 M_w 8.8 Maule earthquake [1] and (ii) physically plausible inter-plate locking models. Together they represent 10 different seismic scenarios and constitute the base to generate synthetic seismograms (Fig.1). The geometry of the 2010 Maule rupture model was matched in North Chile to fill in the existing seismic gap [2]. This was done by adjusting the Maule geometry to the local geometry of plates in the north consistent with the Slab 1.0 model [3]. In total, four seismic scenarios were generated from the original slip distribution of Maule, of which three included artificial variations of plate slip. In addition, three locking models were used to generate other six scenarios with single and multiple patches of slip. All these models are then used to estimate low-frequency synthetic ground motions using the methodology described herein [1]. Variations on selected mean rupture velocity and slip rise time were later introduced to analyze uncertainty on spectral values due to low-frequency motions. Responses considered were peak ground displacement PGD, displacement spectra S_d, and pseudo-acceleration spectra S_a.

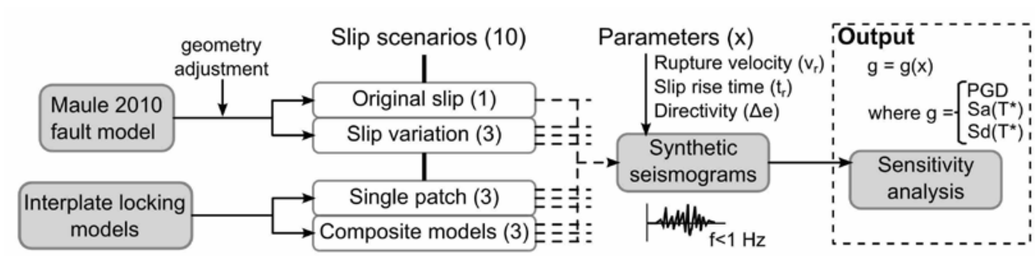

Fig. 1 – Schematic flow chart describing the methodology used

2. The 2010 Maule earthquake on North Chile

The North Chile seismic gap extends approximately from South Peru (Latitude 15.5°S) to the Mejillones peninsula (Latitude 23°S), evidencing more than 500 km of lack of megathrust earthquakes since the last $M_w \geq 8.5$, 1868 and 1877 earthquakes [2]. The 2014 M_w 8.1 Pisagua earthquake ruptured only about 20% of this seismic gap [4], evidencing that risk for a large earthquake to strike this area is still high. The locking models used herein have been developed based on the accumulated seismic inter-plate coupling along the gap [5]. These physical models were used to build 6 plausible seismic scenarios.

Only as a first attempt to bound uncertainty for a future $M_w \geq 8.5$ in the region, the finite-fault rupture model previously derived for the 2010 Maule earthquake [1] was adapted to the plate geometry in north Chile to fill in the existing seismic gap. This is represented by the shade area in Fig.2a. In order to follow the local geometry of the plate boundary, the original fault plane was divided into two quadrilateral (trapezoidal) areas, each with one main patch of slip (Fig.2b). To make the model consistent with the slab geometry, the dip and strike angles of each sub-fault were modified according to the Slab 1.0 model [3], assuming variable dip angles along the dip-down direction of the fault. The strike was defined as 324.5° and 357.5° for the north and south large fault surfaces, respectively. The updip and downdip limits of these faults were fixed at 5 km and 50-55 km depth, respectively, which is consistent with previous studies [5]. Although a minor variation on the original slip distribution was required in adjusting the geometry of the fault, the seismic moment $M_o = 1.85 \times 10^{22}$ Nm and moment magnitude M_w 8.8 of this scenario still represent the one estimated previously with InSAR data [1].

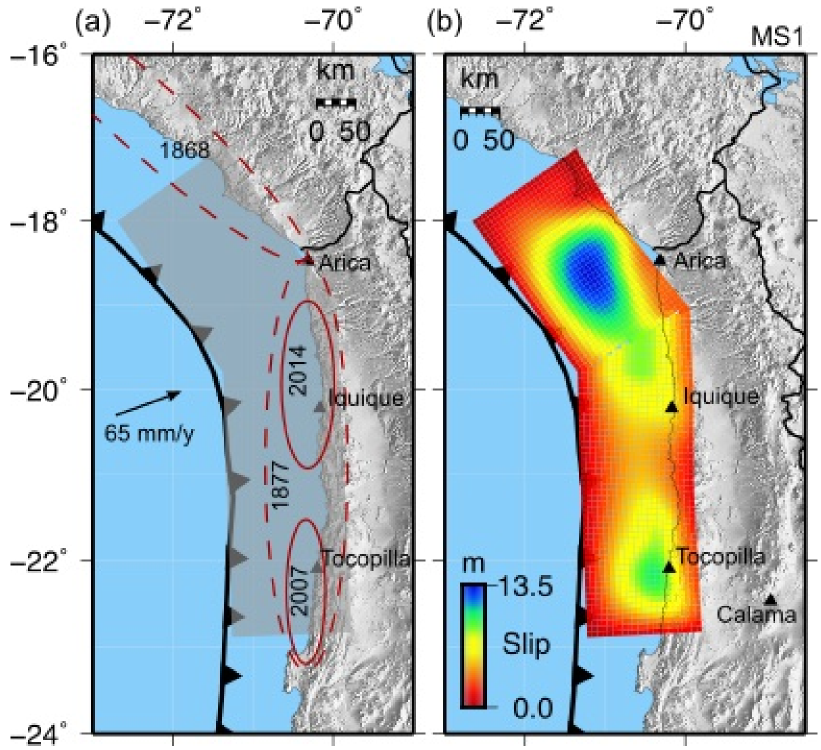

Fig. 2 – Definition of the first set of rupture models: (a) Dashed line ellipses represent rupture of the 1868 and 1877 earthquakes, while solid line ellipses the rupture of the 2014 M_w 8.1 Pisagua and the 2007 M_w 7.7 Tocopilla earthquakes—shade area represents the geometry of the fault model defined; (b) artificial slip model scenario built from 2010 Maule earthquake finite fault rupture model (MS1).

3. Seismic scenarios

Considering the geometry described above, ten seismic scenarios with different slip distributions were defined based on the Maule 2010 estimated slip model [1] and the locking models for the north Chile seismic gap [5,6]. As explained earlier, the first seismic scenario defined considered the same slip distribution estimated for the 2010 Maule earthquake [1] with some minor adjustments for the new geometry (Fig.2b, scenario MS1). Furthermore, three seismic scenarios are obtained by creating some variations explained later on the original slip distribution on the MS1 while keeping the same geometry overall. These scenarios are called hereafter MS2, MS3 and MS4. Moreover, the interplate locking estimation leads to the definition of three additional seismic scenarios near to the cities of Arica (LS2), Tocopilla (LS3), and Iquique (LS5). Each one of these models have only one patch of slip, and the combination of them produces the three final scenarios with two (LCS1 – LCS2) and three patches of slip (LCS3). The latter assume that the rupture of one locking zone could trigger a larger rupture along the gap activating the adjacent areas. All scenarios are consistent with the Slab 1.0 model [3].

Artificial seismic scenarios MS2, MS3, and MS4 derived from the 2010 Maule slip model are shown in Fig.3. Different slip distributions were built by replacing each patch of slip with a two-dimensional Gaussian distribution with specified variance and maximum slip at the center of the corresponding patch. This allows the parametrization of the slip distributions. For instance, the MS2 scenario (Fig.3a) was obtained by modifying the south slip asperity to get a larger local maximum slip of 11.9 m, while keeping the north slip patch equal to the original model. Likewise, the MS3 scenario (Fig.3b) was built by replacing the north slip asperity by a local distribution with elliptical shape and maximum slip of 23.9 m, while preserving the original south slip patch. Also, the MS4 scenario (Fig.3c) combines the south and north slip patches from the MS2 and MS3, respectively. Although there is no physical ground or evidence to support these artificial models, from a design standpoint these models are intuitively useful since they were generated synthetically from a "real" finite fault rupture model and provide information that could help in bounding uncertainty. Therefore, from an epistemic uncertainty standpoint, the results of these models could be combined with the results of other physically driven models using, say, smaller weights.

Shown in Fig.4 are the 6 physical locking models scenarios LS2, LS3, and LS5 (Fig.4a-c) [6], and the compounded models built (Fig.4d-f) by considering that a large earthquake could involve the rupture of two or more slip asperities as it happened during the 2010 Maule earthquake in Chile. When combining locking models, an average slip is considered at the intersection of different rupture segments. Variable dip angle is considered in all these cases according to the Slab 1.0 model [3].

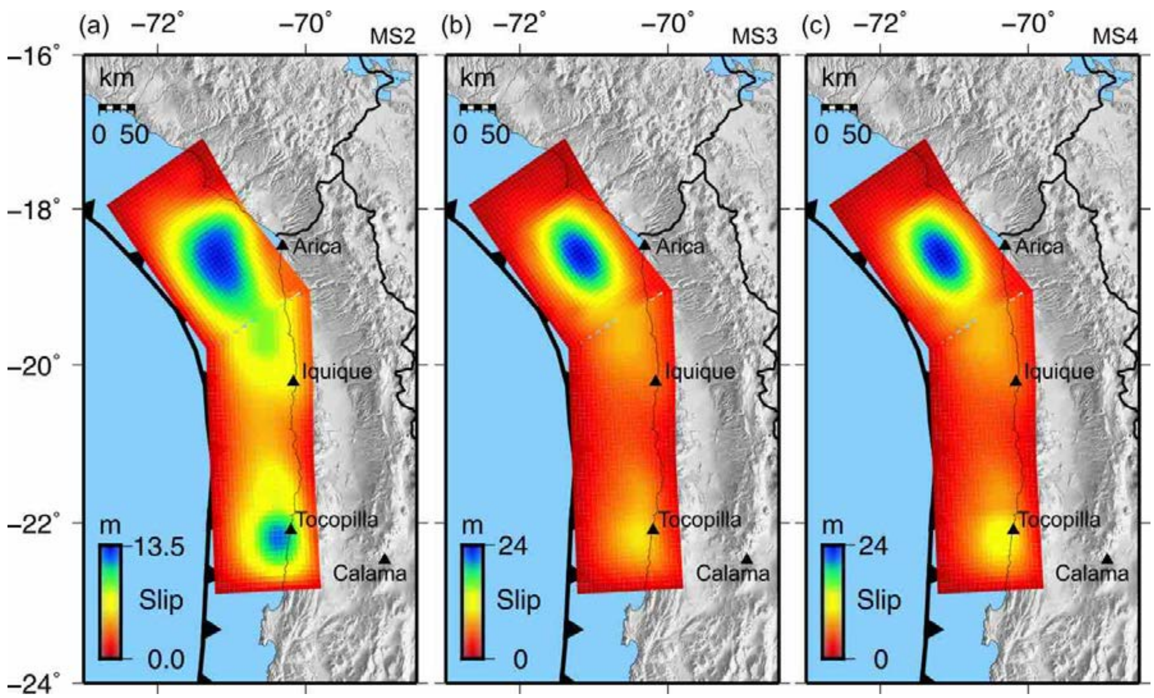

Fig. 3 – Seismic scenarios defined based on the Maule (Chile, 2010) earthquake slip model: (a) MS2: south patch slip variation; (b) MS3: north patch slip variation; and (c) MS4: north and south slip patch variation.

Table 1 shows a summary of the characteristics of the proposed seismic scenarios including the strike and dip angles, maximum slip, seismic moment (M_o) and moment magnitude (M_w). In each case, an homogeneous half-space was considered with a shear modulus of 33 GPa, which is consistent with the value used in previous studies [6, 7].

4. Sensitivity analysis

Low frequency seismograms are determined for each seismic scenario defined using the discrete wavenumber method [9] that computes the Green's functions with a similar methodology to the one detailed elsewhere [1]. The multilayered half-space through which the waves are propagated is defined by the Crust 1.0 model [10], assuming an S-wave attenuation parameter $Q_s = 0.03v_s$ based on previous studies [11, 12], and a P-wave attenuation parameter set by $Q_p = 1.5Q_s$ [13], with v_s the S-wave velocity at each layer. For a given average rupture velocity v_r, the activation time of the slip at the *i-th* sub-fault is defined by $t_a = d_i/v_r$, with d_i the distance between the sub-fault and the earthquake focal point. The focal point for the MS1-4 scenarios is set at the same relative position as in the original 2010 Maule finite fault rupture model, while for the locking model scenarios is defined at the location of maximum slip. The rupture propagation model is considered bilateral (north-south) in all cases. A detailed analysis about the influence of the rupture directivity in the spectral response is still in progress.

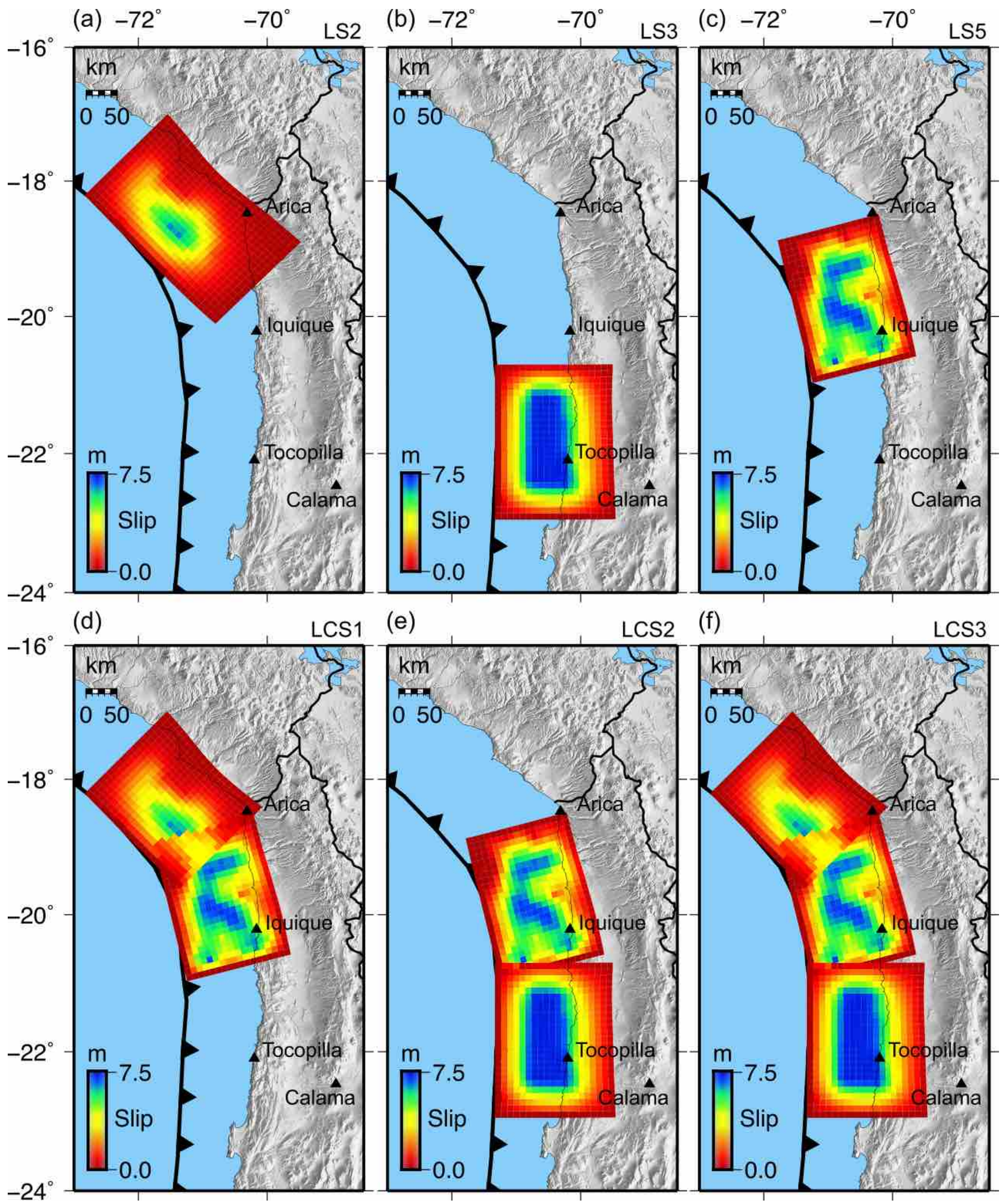

Fig. 4 – Seismic scenarios defined on interplate locking models: (a) LS2: Arica locking model; (b) LS3: Tocopilla locking model; (c) LS5: Iquique locking model; (d) LCS1: Arica plus Iquique compound locking model; (e) LCS2: Iquique+Tocopilla compound locking model; and (f) LCS3: Arica plus Iquique plus Tocopilla compound locking model.

Table 1 – Summary of the seismic scenarios built for this study.

Scenario	# of slip patches	Slip max north (m)	Slip max south (m)	Strike (deg)	Dip (deg)	M_o (N m)	M_w
MS1	2	13.4	10.1	324.5, 357.5	4.3 - 24.8	1.85×10^{22}	8.78
MS2	2	13.4	11.9	324.5, 357.5	4.3 - 24.8	1.88×10^{22}	8.78
MS3	2	23.9	10.1	324.5, 357.5	4.3 - 24.8	2.11×10^{22}	8.82
MS4	2	23.9	11.9	357.5, 324.5	4.3 - 24.8	2.14×10^{22}	8.82
LS2	1	6.47	-	308.5	4.5 - 26	2.61×10^{21}	8.21
LS3	1	7.34	-	358	1.5 - 25.5	5.53×10^{21}	8.43
LS5	1	7.05	-	355	3.7 - 24.2	4.46×10^{21}	8.37
LCS1	2	6.46	7.05	308.5, 355	3.7 - 26	6.97×10^{21}	8.50
LCS2	2	7.05	7.34	355, 358	1.5 - 25.5	1.00×10^{22}	8.60
LCS3	3	6.47	7.34	308.5, 355, 358	1.5 - 26	1.25×10^{22}	8.66

The variability of different spectral response quantities caused by the different scenarios and at the four control sites considered is studied using a deterministic sensitivity analysis. The parameters studied were the average rupture velocity v_r and the slip rise time t_r. Based on the average rupture velocities observed during the 2014 Pisagua earthquake of 2.2 km/s [4], and 2.8 km/s for the Antofagasta (1995) and the Tocopilla (2007) earthquakes [14, 15], nine v_r values were considered in the range 2.2–3.0 km/s to generate synthetic seismograms. Analogously, five values of rise time t_r were considered within the range 2s–10s based on results used in previous studies [16]. For each parameter, the methodology estimates the low-frequency synthetic seismograms using the different values of the control parameter, while keeping all other parameters fixed. Thus, a set of synthetic records is obtained for each seismic scenario; Fig.5 shows for example the synthetic seismograms calculated for the LS5 scenario, i.e. built from the Iquique locking model, using an average rupture velocity v_r = 2.8 km/s and rise time t_r = 5s. In this Figure, the different traces represent the Up-Down, East-West, and North-South components at each of the observation points, which are Iquique, Arica, Tocopilla, and Calama. Difference in the waveforms are quite dramatic depending upon the location of the observation point. Features such as ground displacement offsets are 85cm in the E-W direction for the Iquique station, while such offsets are essentially zero in the Tocopilla and Calama stations. Peak ground displacements also flip from the E-W to the N-S direction for the Arica station. There are several other characteristics of these waveforms that for the sake of brevity are not detailed here.

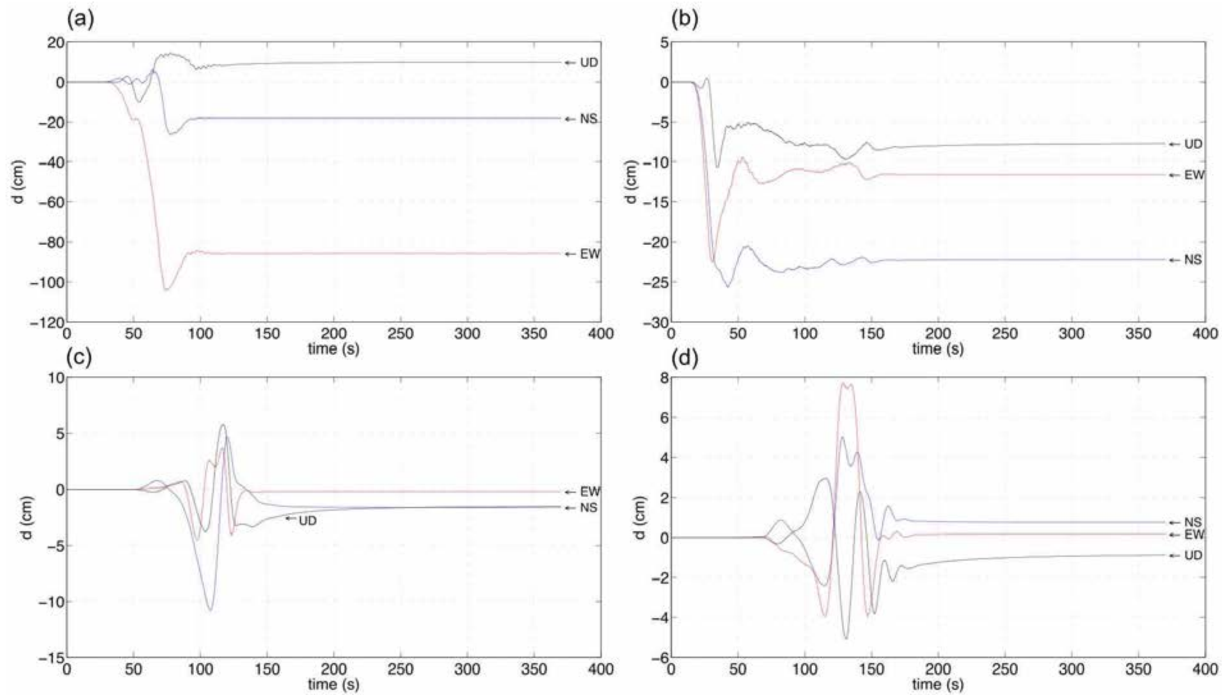

Fig. 5 – Realizations of synthetic seismograms obtained at four observation points for the LS5 scenario using v_r = 2.8 km/s, t_r = 5s, and epicenter at 19˚W 71˚S: (a) Iquique; (b) Arica; (c) Tocopilla; and (d) Calama stations. NS and EW refer to north-south and east-west direction, respectively. Location of stations is shown on Fig.4.

All computations presented herein are very time consuming, so to construct the complete functional dependency of design variables we used a second order Taylor approximation. The approximation uses the numerically estimated first and second order derivatives in the vicinity of each v_r and t_r value. In general terms, this approximation may be written as

$$r(\boldsymbol{p}) = r(\overline{\boldsymbol{p}}) + (\nabla r)^T_{,\boldsymbol{p}}\,(\boldsymbol{p}-\overline{\boldsymbol{p}}) + \frac{1}{2}(\boldsymbol{p}-\overline{\boldsymbol{p}})^T\nabla(\nabla r_{,\boldsymbol{p}})_{,\boldsymbol{p}}(\boldsymbol{p}-\overline{\boldsymbol{p}}) + o(\|(\boldsymbol{p}-\overline{\boldsymbol{p}})\|^3) \quad (1)$$

where "r" represents any scalar response quantity of the ground motion, such as PGD; $\boldsymbol{p}$ represents the vector of parameters considered in the finite fault rupture model; $(\nabla r)^T_{,\boldsymbol{p}}$ is the gradient of the response relative to a change in the vector of parameters $\boldsymbol{p}$; and $o(\|(\boldsymbol{p}-\overline{\boldsymbol{p}})\|^3)$ is a term of order cubed in the Taylor expansion. This expression can also be used to compute the mean and variance of the response "r" in case one considers the finite fault rupture parameter vector as a random variable, i.e.

$$E[r(\boldsymbol{p})] \approx r(\overline{\boldsymbol{p}}) + (\nabla r)^T_{,\boldsymbol{p}}\,E[\boldsymbol{p}-\overline{\boldsymbol{p}}] + \frac{1}{2}\nabla(\nabla r_{,\boldsymbol{p}})_{,\boldsymbol{p}}E[(\boldsymbol{p}-\overline{\boldsymbol{p}})^T(\boldsymbol{p}-\overline{\boldsymbol{p}})] \quad (2)$$

where E represents the expected value of quantity $(\cdot)$.

Shown in Fig. 6 is the peak ground displacement, PGD, for each of the 10 earthquake scenarios in each of the four observation stations as a function of the average rupture velocity v_r and assuming a fixed rise time value t_r = 5s. For a given scenario, Green's functions were computed for each sub-fault and synthetic seismograms were obtained at each observation site (station) by convolving these signals. The procedure is repeated for the different values of v_r, thus enabling to estimate PGD as a function of v_r for each scenario. It is apparent that the scenarios that produce higher values of PGD at each site are those that have large values of slip closer to the corresponding station. For example, for the Arica station (Fig.6a) in the EW direction, the larger values of PGD are obtained for the MS3 and MS4 scenarios, which reach PGDs of almost 2m for higher rupture velocities. A general trend is that PGD increases with rupture velocity; furthermore, in most cases PGD is larger in the EW direction than in the NS direction. Although in some cases PGD varies as little as 1-2% as v_r increases from 2.2 to 3 km/s, for the locking models the PGD more than doubles if v_r = 3 km/s instead of 2.2 km/s. The scenarios that produce less variation on PGD, say less than 10%, are those built from the 2010 Maule earthquake. In general, Arica presents the largest variations with 78% and 72% increase in PGD in the NS and EW directions, respectively. The lowest average variation in PGD is obtained for Iquique and Tocopilla that in average reach 30% and 52% approximately in the NS and EW directions, respectively.

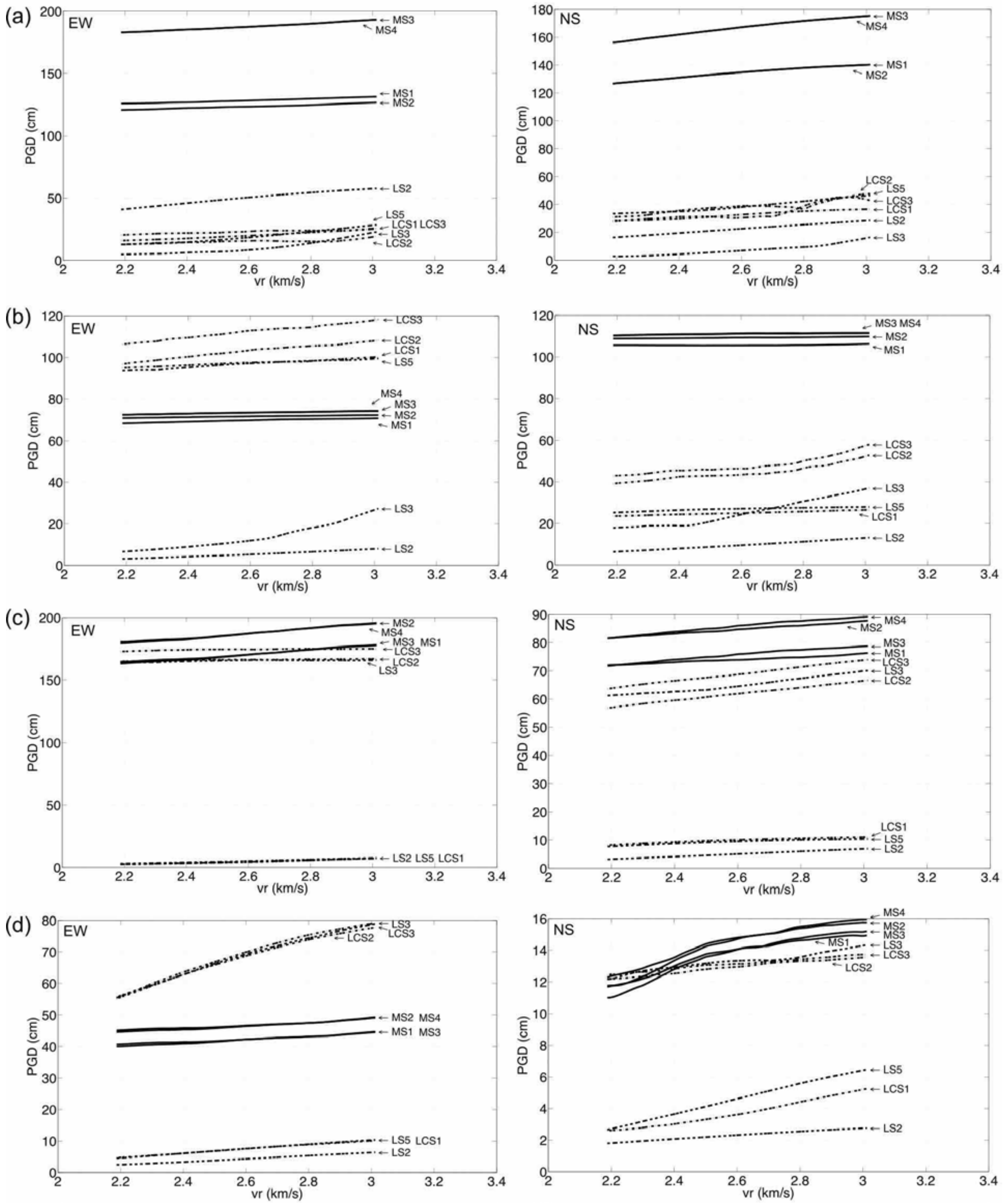

Fig. 6 – Estimation of the PGD as a function of v_r, t_r = 5s, and stations: (a) Arica; (b) Iquique; (c) Tocopilla; and (d) Calama—NS and EW refer to north-south and east-west directions, respectively.

The sensitivity to slip rise time was studied using Green's functions with values t_r = 2, 4, 6, 8, and 10s. These values were used to obtain a set of synthetic seismograms at each site for all the scenarios considered. The Green's functions obtained for each t_r value were convolved using a rupture model with fixed average rupture velocity v_r = 2.8 km/s. This computational process is very demanding, especially in larger scenarios with many sub-fault elements, for which the Green's function needs to be calculated. Spectral responses are obtained for each rise time value thus leading to a PGD function of t_r, a set of displacement spectra S_d and pseudo-acceleration spectra S_a for each site.

As an example, Fig.7 shows PGD obtained for different values of rise time (t_r = 2–10s) using the LS5 seismic scenario at all four stations: Iquique, Arica, Tocopilla and Calama. Point markers show the discrete values of PGD obtained, while curves are estimations of the PGD function using a cubic spline interpolation. Each plot shows the results for the NS and EW directions, using solid and dashed lines, respectively. It is apparent for all sites that as rise time increases, PGD decreases. This reduction is as large as 48% in Calama in the NS direction and 63% in Tocopilla in the EW direction when t_r increases from 2s to 10s. The overall higher values of PGD occur in Iquique (Fig.7b) and are consistent with the distance of this site to the patch of maximum slip in the LS5 scenario. For this scenario, the smallest variation of PGD is 7% obtained in Iquique in the EW direction.

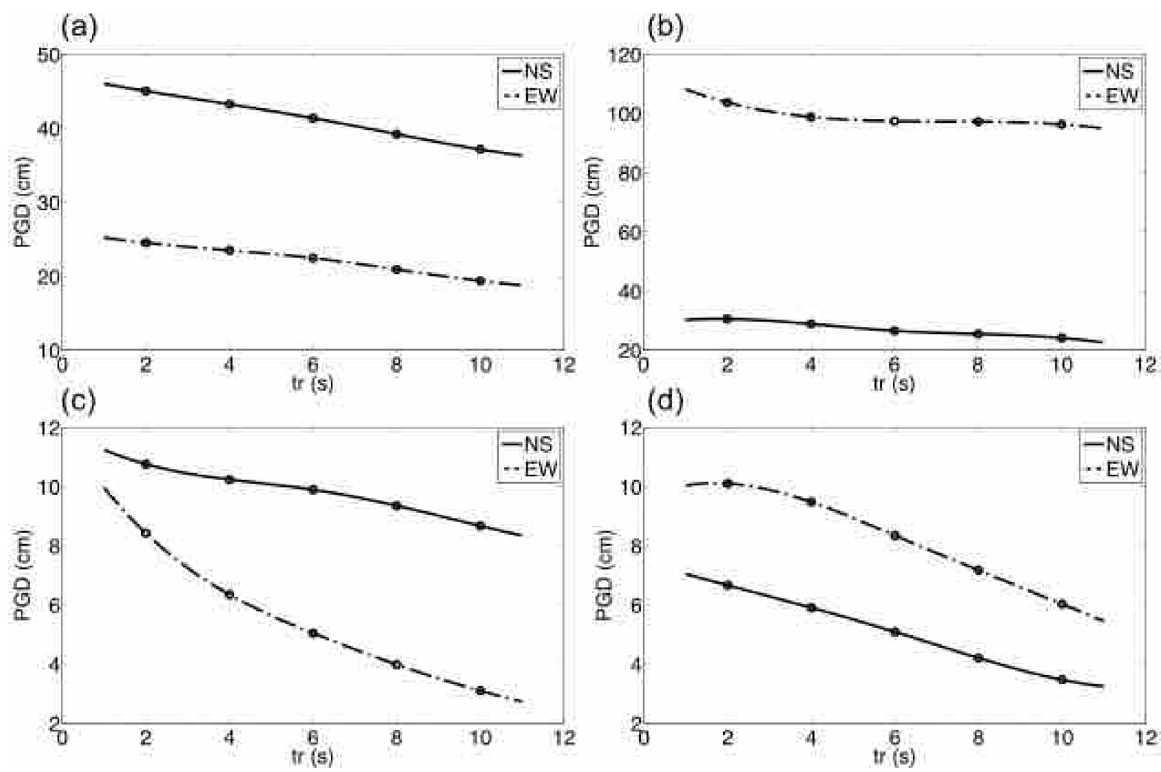

Fig. 7 – Estimation of PGD function of t_r using v_r = 2.8 km/s for scenario LS5 and stations: (a) Arica; (b) Iquique; (c) Tocopilla; and (d) Calama.

The displacement and pseudo-acceleration spectra obtained using the LS5 scenario and rise time t_r = 2s–10s at Iquique are shown in Fig.8. As the method used does include the high frequencies accurately [17], the spectra are analyzed only for periods T$\geq$1s. This figure shows that as the slip rise-time value increases, the spectral response decreases. This suggests that shorter values of slip rise-time might lead to higher seismic demands in flexible long period structures. Similar results were obtained in all four control stations considered regardless of the distance to the fault.

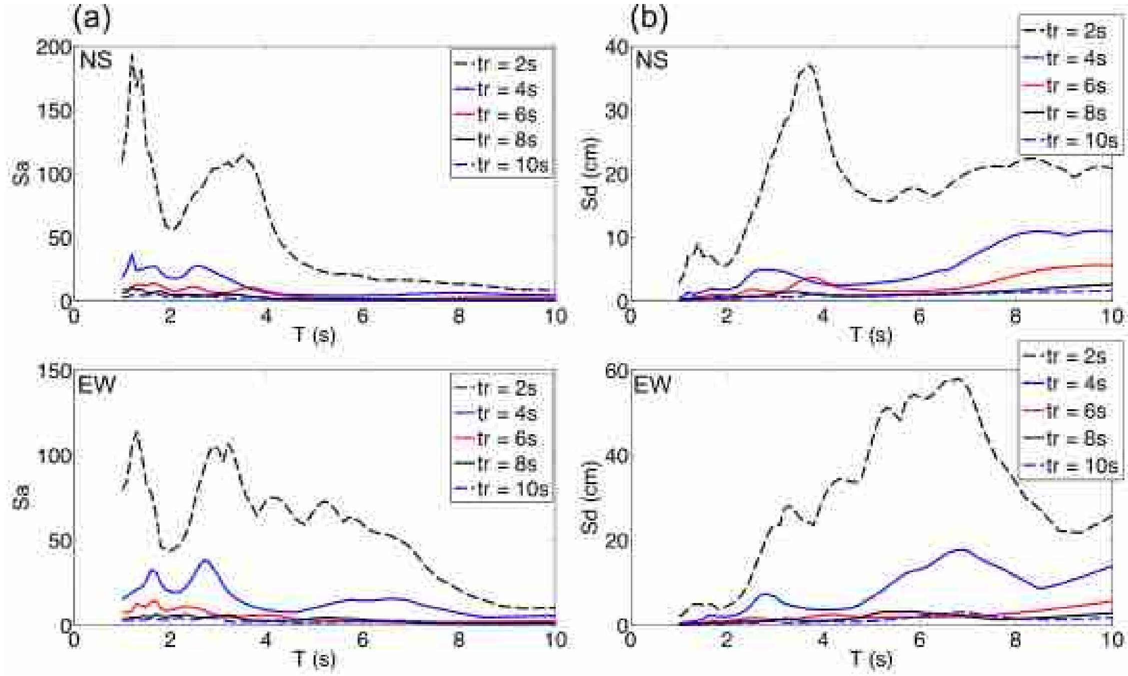

Fig. 8 – Response spectra obtained using t_r = 2s–10s for the LS5 scenario at Iquique: (a) Pseudo-acceleration spectra; and (b) displacement spectra for v_r = 2.8 km/s.

5. Conclusions

The capacity to generate diverse seismic scenarios using available information from past earthquakes and seismological data of rupture models and newer seismic coupling studies may be a great resource for better characterizing the seismic demand for structural engineering purposes.

This research on the lower frequency component of ground motions led to the conclusion that the effect of the average rupture velocity v_r on the seismic demand PGD varies between scenarios, and depends on the distance of the station to the rupture. The global trends of the relationship between PGD and v_r show that larger values of v_r lead to higher values of PGD.

Also, from the response spectra obtained using the slip rise-time analysis, it was shown that the response of long period structures is particularly sensitive to variations in this parameter. Previous studies have shown that this parameter may vary as widely as 1.3s to 20s [16, 18], which evidences the need to develop detailed studies for the value of t_r in Chilean earthquakes. Meanwhile, the estimation of low frequency seismograms from artificial seismic scenarios should be done carefully by considering a conservative approach regarding this parameter, i.e. small values of t_r that lead to higher seismic demand in long period structures.

As future work, this analysis will be expanded to analyze the influence of the epicenter location and rupture directivity on spectral responses obtained from the seismic scenarios presented herein.

6. Acknowledgements

This research has been sponsored by grants National Research Center for Integrated Natural Disaster Management (CIGIDEN), CONICYT/FONDAP #15110017 and Fondecyt Grant 1141187. The authors are very grateful for this support.

7. References

[1] C. Fortuño, J. C. de la Llera, C. W. Wicks, and J. a. Abell, “Synthetic Hybrid Broadband Seismograms Based on InSAR Coseismic Displacements,” *Bull. Seismol. Soc. Am.*, vol. 104, no. 6, pp. 2735–2754, Nov. 2014.

[2] D. Comte and M. Pardo, “Reappraisal of Great Historical Earthquakes in the Northern Chile and Southern Peru Seismic Gaps,” *Nat. Hazards*, vol. 4, pp. 23–44, 1991.

[3] G. P. Hayes, D. J. Wald, and R. L. Johnson, “Slab1.0: A three-dimensional model of global subduction zone geometries,” *J. Geophys. Res.*, vol. 117, Jan. 2012.

[4] T. Lay, H. Yue, E. E. Brodsky, and C. An, “The April 1, 2014 Iquique, Chile Mw 8.1 earthquake rupture sequence,” *Geophys. Res. Lett.*, vol. 41, no. 11, pp. 1–28, 2014.

[5] J. Cortés-Aranda, G. González, D. Rémy, and J. Martinod, “Normal upper plate fault reactivation in northern Chile and the subduction earthquake cycle: From geological observations and static Coulomb Failure Stress (CFS) change,” *Tectonophysics*, vol. 639, pp. 118–131, 2015.

[6] M. N. Shrivastava, J. González-Carrasco, C. Fuentes, G. González, P. Salazar, G. A. Yáñez, and J. C. de la Llera, “Deterministic seismic hazard assessment for the southern Peru and northern Chile segment of the Andean subduction zone,” in *AGU Fall Meeting, San Francisco, EEUU*, 2015.

[7] M. Béjar-Pizarro, A. Socquet, R. Armijo, D. Carrizo, J. Genrich, and M. Simons, “Andean structural control on interseismic coupling in the North Chile subduction zone,” *Nat. Geosci.*, vol. 6, no. 6, pp. 462–467, Apr. 2013.

[8] M. Motagh, B. Schurr, J. Anderssohn, B. Cailleau, T. R. Walter, R. Wang, and J.-P. Villotte, “Subduction earthquake deformation associated with 14 November 2007, Mw 7.8 Tocopilla earthquake in Chile: Results from InSAR and aftershocks,” *Tectonophysics*, vol. 490, no. 1–2, pp. 60–68, Jul. 2010.

[9] L. Zhu and L. A. Rivera, “A note on the dynamic and static displacements from a point source in multilayered media,” *Geophys. J. Int.*, vol. 148, pp. 619–627, 2002.

[10] G. Laske, G. Masters, Z. Ma, and M. Pasyanos, “Update on CRUST1.0 - A 1-degree Global Model of Earth’s Crust,” *Geophys. Res. Abstr.*, vol. 15, 2013.

[11] S. C. Myers, S. Beck, G. Zandt, and T. Wallace, “Lithospheric-scale structure across the Bolivian Andes from tomographic images of velocity and attenuation for P and S waves,” *J. Geophys. Res.*, vol. 103, no. B9, pp. 21233–21252, 1998.

[12] J. C. Stachnik, G. a. Abers, and D. H. Christensen, “Seismic attenuation and mantle wedge temperatures in the Alaska subduction zone,” *J. Geophys. Res. Solid Earth*, vol. 109, 2004.

[13] P. Liu, R. J. Archuleta, and S. H. Hartzell, “Prediction of Broadband Ground-Motion Time Histories: Hybrid Low/High- Frequency Method with Correlated Random Source Parameters,” *Bull. Seismol. Soc. Am.*, vol. 96, no. 6, pp. 2118–2130, Dec. 2006.

[14] B. Delouis, T. Monfret, L. Dorbath, M. Pardo, L. Rivera, D. Comte, and H. Haessler, “The Mw = 8.0 Antofagasta (Northern Chile) Earthquake of 30 July 1995: A Precursor to the End of the Large 1877 Gap,” *Bull. Seismol. Soc. Am.*, vol. 87, no. 2, pp. 427–445, 1997.

[15] B. Delouis, M. Pardo, D. Legrand, and T. Monfret, “The Mw 7.7 Tocopilla earthquake of 14 November 2007 at the Southern edge of the Northern Chile seismic gap: Rupture in the deep part of the coupled plate interface,” *Bull. Seismol. Soc. Am.*, vol. 99, no. 1, pp. 87–94, 2009.

[16] A. Frankel, “Rupture History of the 2011 M 9 Tohoku Japan Earthquake Determined from Strong-Motion and High-Rate GPS Recordings: Subevents Radiating Energy in Different Frequency Bands,” *Bull. Seismol. Soc. Am.*, vol. 103, no. 2B, pp. 1290–1306, May 2013.

[17] L. Hutchings and G. Viegas, “Application of Empirical Green’s Functions in Earthquake Source, Wave Propagation and Strong Ground Motion Studies,” in *Earthquake Research and Analysis - New Frontiers in seismology*, S. D’Amico, Ed. Intech, 2012, pp. 87–140.

[18] A. Frankel, “A Constant Stress-Drop Model for Producing Broadband Synthetic Seismograms: Comparison with the Next Generation Attenuation Relations,” *Bull. Seismol. Soc. Am.*, vol. 99, no. 2A, pp. 664–680, Apr. 2009.